Structural prediction of Fe-Mg-O compounds at super-Earth's pressures

Yimei Fang,[1] Yang Sun,[1,2,*] Renhai Wang,[3] Feng Zheng,[4] Feng Zhang,[2] Shunqing Wu,[1,†] Cai-Zhuang Wang,[2] Renata M. Wentzcovitch,[5,6,7,8,‡] and Kai-Ming Ho[2]

[1]*Department of Physics, OSED, Key Laboratory of Low Dimensional Condensed Matter Physics (Department of Education of Fujian Province), Jiujiang Research Institute, Xiamen University, Xiamen 361005, China*
[2]*Department of Physics, Iowa State University, Ames, Iowa 50011, USA*
[3]*School of Physics and Optoelectronic Engineering, Guangdong University of Technology, Guangzhou 510006, People's Republic of China*
[4]*School of Science, Jimei University, Xiamen 361021, China*
[5]*Department of Applied Physics and Applied Mathematics, Columbia University, New York, New York 10027, USA*
[6]*Department of Earth and Environmental Sciences, Columbia University, New York, New York 10027, USA*
[7]*Data Science Institute, Columbia University, New York, New York 10027, USA*
[8]*Lamont-Doherty Earth Observatory, Columbia University, Palisades, New York 10964, USA*

(Received 14 July 2023; accepted 11 October 2023; published 6 November 2023)

Terrestrial exoplanets are of great interest for being simultaneously similar to and different from Earth. Their compositions are likely comparable to those of solar-terrestrial objects, but their internal pressures and temperatures can vary significantly with their masses/sizes. The most abundant nonvolatile elements are O, Mg, Si, Fe, Al, and Ca, and there has been much recent progress in understanding the nature of magnesium silicates up to and beyond ≈3 TPa. However, a critical element, Fe, has yet to be systematically included in materials discovery studies of potential terrestrial planet-forming phases at ultrahigh pressures. Here, using the adaptive genetic algorithm crystal structure prediction method, we predict several unreported stable crystalline phases in the binary Fe-Mg and ternary Fe-Mg-O systems up to pressures of 3 TPa. The analysis of the local packing motifs of the low-enthalpy Fe-Mg-O phases reveals that the Fe-Mg-O compound favors a bcc motif under ultrahigh pressures. In addition, oxygen enrichment is conducive to lowering the enthalpies of the Fe-Mg-O phases. Our results extend the current knowledge of structural information of the Fe-Mg-O system to exoplanet pressures.

DOI: 10.1103/PhysRevMaterials.7.113602

I. INTRODUCTION

The past two decades have witnessed a rapid increase in the number of discovered exoplanets, among which terrestrial-type exoplanets with masses under $10M_\oplus$ ($M_\oplus$: Earth's mass), frequently referred to as "super-Earth," are of particular interest for their similarities to and differences from Earth and their potential to host life. Among other factors, this life-host potential depends on its internal structure, particularly the existence of a planetary core able to produce a radiation-shielding magnetic field at the surface. By analyzing the spectroscopic features of the atmospheres of white dwarfs that are polluted by exoplanetary accretions, Young and coworkers reached the conclusion that the primary nonvolatile elements of terrestrial exoplanets are expected to be the same as those of solar terrestrial planets, i.e., O, Mg, Si, Fe, Al, and Ca [1,2]. An exoplanet's internal structure is also expected to consist of an iron-rich metallic core and a surrounding silicate mantle (see, e.g., Refs. [3,4]), just like the solar terrestrial ones. However, the internal pressure in a large terrestrial planet can be much higher, e.g., approximately 1.2 TPa at the core-mantle boundary of a planet with $\approx 12M_\oplus$ [3].

Currently, considerable theoretical efforts have focused on exploring Mg-Si-O compounds and investigating their post-post-perovskite phase transitions [3,5–10] at exoplanet conditions. However, Fe is one of the most abundant elements on terrestrial planets, and it must combine with the other rock-forming elements to form Fe-bearing compounds. While Fe is hardly miscible with Mg at ambient conditions, Fe and Mg have complete solubility in oxides even at zero pressure. In addition, given that high pressure facilitates the mixture of Fe/Mg compounds [11–14], it is reasonable that abundant Fe-Mg-O ternary phases should exist under exoplanetary conditions. Although the thermodynamic and spin crossover properties [15–17] in ferropericlase (i.e., B1-type $Mg_{1-x}Fe_xO$) at Earth's lower-mantle conditions and super-Earth's mantle conditions (B2-type $Mg_{1-x}Fe_xO$) [18–20] have been extensively studied, relatively less attention has been paid to the Fe-Mg-O phases with other metal-to-oxygen ratios at exoplanetary pressures.

Here, using the adaptive genetic algorithm (AGA) [21] we perform structure predictions for the ternary Fe-Mg-O phases with variable compositions at 1 and 3 TPa. Two unreported compounds, i.e., $FeMgO_3$ and $FeMg_3O_4$, are found to be stable. The analysis of the local packing motifs of the Fe-Mg-O phases with lower enthalpies leads us to conclude that the Fe-Mg-O system favors a bcc-type motif under ultrahigh pressures. Additionally, we find that an O-rich environment is beneficial to lowering the enthalpies of the Fe-Mg-O phases.

*Corresponding author: yangsun@xmu.edu.cn
†Corresponding author: wsq@xmu.edu.cn
‡Corresponding author: rmw2150@columbia.edu

While the effects of temperature are not included here, our present paper provides ample structural and motif information for future analysis of the thermodynamic properties of these compounds at high-pressure and high-temperature conditions.

II. COMPUTATIONAL METHODS

The AGA method [21] combines the efficiency of structure exploration by classical potential calculations and the accuracy of density functional theory (DFT) calculations adaptively and iteratively. In the current AGA searches for Fe-Mg-O phases, unit cells containing up to 4 f.u. were used, and initial atomic positions were randomly generated without any assumption on the symmetry. Structure searches were performed at 1 and 3 TPa, and the enthalpy was used as the selection criteria for optimizing the candidate structures pool. We kept the pool size in the current searches to 128 structures. At each genetic algorithm (GA) generation, 32 (i.e., a quarter of the pool size) new structures are produced from the parent structure pool through the mating procedure described in Ref. [22], and are updated to the candidate pool as parent structures for the next generation. The structure search was carried out for 600 consecutive GA generations using a specific auxiliary interatomic potential. After the GA search, 16 lowest-enthalpy structures were selected for first-principles calculations to obtain the enthalpies, forces, and stresses to readjust the potential parameters of the classical auxiliary potential for the next GA search. We performed 60 adaptive iterations to obtain the final structures for a given chemical composition.

Here, interatomic potentials based on the embedded-atom method (EAM) [23] were chosen as the classical auxiliary potential. Within the EAM, the total energy of an N-atom system takes the form of

$$E_{\text{total}} = \frac{1}{2}\sum_{i,j(i\neq j)}^{N} \phi(r_{ij}) + \sum_i F_i(n_i), \tag{1}$$

where $\phi(r_{ij})$ is the pair repulsion between atoms i and j with a distance of r_{ij}. $F_i(n_i)$ is the embedded term with electron density term $n_i = \sum_{j\neq i} \rho_j(r_{ij})$ at the site occupied by atom i. The fitting parameters in the EAM formula for the Fe-Mg-O system are determined as follows: the parameters for Fe-Fe and Mg-Mg interactions were taken from the literature [24], and the other pair interactions (i.e., O-O, Fe-Mg, Fe-O, and Mg-O) were modeled by the Morse function:

$$\phi(r_{ij}) = D[e^{-2\alpha(r_{ij}-r_0)} - 2e^{-\alpha(r_{ij}-r_0)}], \tag{2}$$

where D, α, and r_0 are the fitting parameters. For O atoms, the density function was modeled by an exponentially decaying function

$$\rho(r_{ij}) = \alpha \exp[-\beta(r_{ij} - r_0)], \tag{3}$$

where α and β are the fitting parameters; the embedding function was expressed by

$$F(n) = F_0[1 - \gamma \ \text{In}\ n]n^{\gamma} \tag{4}$$

with fitting parameters F_0 and γ, as proposed by Benerjea and Smith in Ref. [25]. For Fe and Mg, the parameters of the density function and embedding function were also taken from Ref. [24].

During the AGA run, the potential parameters were adjusted adaptively by fitting to the selected structures' DFT-calculated enthalpies, forces, and stresses. The fitting procedure was conducted by adopting the force-matching method with a stochastic simulated annealing algorithm as implemented in the POTFIT code [26,27].

The first-principles calculations were carried out within DFT as implemented in the QUANTUM ESPRESSO code [28,29]. The exchange-correlation functional was treated with the non-spin-polarized generalized-gradient approximation as parametrized by the Perdew-Burke-Ernzerhof formula [30]. We used the pseudopotentials of Fe and Mg that were generated, tested, and previously used in Ref. [31]. The pseudopotentials for Fe and O were generated with the valence electronic configuration of $3s^2\,3p^6\,3d^{6.5}\,4s^1$ and $2s^2\,2p^4$. Five configurations, including $3s^2\,3p^0$, $3s^1\,3p^1$, $3s^1\,3p^{0.5}\,3d^{0.5}$, $3s^1\,3p^{0.5}$, and $3s^1\,3d^1$, with decreasing weights 1.5, 0.6, 0.3, 0.3, and 0.2, respectively, are used for Mg. The pseudopotentials were also used in a few studies at terapascal pressures [5,8,32]. A kinetic-energy cutoff of 50 Ry for wave functions and one of 500 Ry for potentials were used. The Brillouin-zone integration was performed over a k-point grid of $2\pi \times 0.03$ Å^{-1} in the structure refinement. Convergence thresholds are 0.01 eV/Å for the atomic force, 0.05 GPa for the pressure, and 1×10^{-5} eV for the total energy.

III. RESULTS AND DISCUSSION

A. Phase stability

We systematically investigate the phase stabilities of several stoichiometric $Fe_xMg_yO_z$ compounds predicted by the AGA search. We assign integer values from 1 to 4 to x, y, and z. This results in 64 different Fe, Mg, and O compositions. After removing redundant compositions, we searched 55 distinct stoichiometries of $Fe_xMg_yO_z$ with up to 56 atoms at 1 and 3 TPa. The formation enthalpy per atom (H_f) of a $Fe_xMg_yO_z$ phase at a given pressure is expressed as

$$H_f = \frac{H_{\text{Fe}_x\text{Mg}_y\text{O}_z} - (xH_{\text{Fe}} + yH_{\text{Mg}} + zH_{\text{O}})}{x+y+z}, \tag{5}$$

where $H_{\text{Fe}_x\text{Mg}_y\text{O}_z}$ stands for the enthalpy of the $Fe_xMg_yO_z$ phase, and H_{Fe}, H_{Mg}, and H_{O} stand for the enthalpies of pure Fe, Mg, and O elements, respectively. We can construct the ternary convex hull based on the formation enthalpies of all the searched phases. Here, the convex hull is a hypersurface in compositional space that connects all elementary, binary, and ternary compounds that are thermodynamically stable against decomposition [33]. A $Fe_xMg_yO_z$ phase is identified as stable if it lies on the vertex of the convex hull. If a $Fe_xMg_yO_z$ phase is above the convex hull, it is metastable and should decompose to the stable phases under thermodynamical equilibrium.

To construct the ternary convex hull, we first address the ground-state structures of elementary and binary phases on the phase diagram. Previous studies have investigated elementary and binary phases consisting of Fe, Mg, and O. It has been reported that at 500 GPa, elementary Fe adopts the hcp structure [34]. Our calculations show that the hcp phase of Fe remains as the ground state at both 1 and 3 TPa compared to

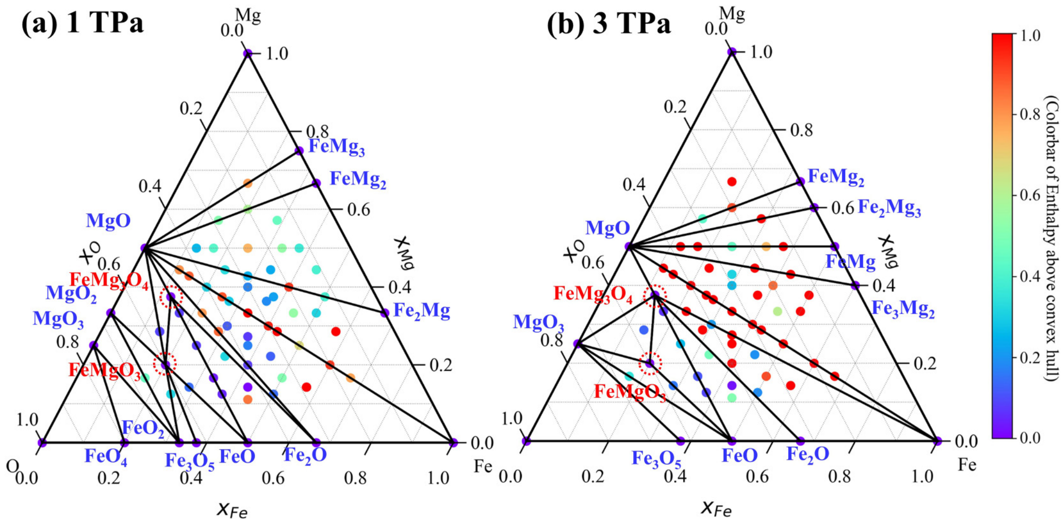

FIG. 1. Ternary phase diagram of the Fe-Mg-O system at (a) 1 TPa and (b) 3 TPa. The points marked by red dashed circles represent the ground-state $Fe_xMg_yO_z$ phases. The colors of solid circles indicate the relative formation enthalpy in eV/atom to the convex hull.

the bcc phase. In the pressure range of our interest, Mg undergoes a phase transition from the simple hexagonal structure (sh) to the simple cubic (sc) structure at 1.07 TPa [9,35,36]. Consequently, the sh and sc structures are the reference phases at 1 and 3 TPa, respectively. Elementary oxygen exhibits a variety of phases within a range of pressures from 0.25 to 10 TPa [37]. By performing structural optimization for these phases at 1 and 3 TPa, we find that the $I4_1/acd$ phase is the ground-state phase at 1 TPa and the *Cmcm* phase with zigzag-chain-like structure is the ground state at 3 TPa. Note that Ref. [37] indicates $I4_1/acd$ is a metastable state at 1 TPa and it only becomes the ground state at 2 TPa. This discrepancy may stem from the different pseudopotentials used in the calculations. Our pseudopotential was generated by the Vanderbilt method [38]. It had been tested in a few studies at high pressures [5,8], while Ref. [37] used the projector augmented wave pseudopotentials shipped with VASP software.

For the reference binary phases, the stable Mg-O compounds under high pressures have been extensively explored by Niu *et al.* [9] and Zhu *et al.* [35]. MgO, MgO_2, and MgO_3 phases are found to be stable ground states at 1 TPa. While the MgO and MgO_3 structures remain stable at 3 TPa, the MgO_2 phase decomposes into MgO and MgO_3 at 1.43 TPa. Therefore, we use MgO, MgO_2, and MgO_3 as the reference at 1 TPa, while we use only MgO and MgO_3 at 3TPa. Weerasinghe *et al.* [34] predicted several stable structures with different stoichiometries for up to 500 GPa for the Fe-O system. By extending their calculation to 1 and 3 TPa, we found that four of their predicted structures, i.e., FeO, FeO_2, FeO_4, and Fe_2O, are still stable ground states at 1TPa, while only FeO, Fe_2O, and FeO_2 remain ground states up to 3 TPa [32]. In addition, we recently identified two different stable Fe_3O_5 phases at 1 and 3TPa [32]. Gao *et al.* [13] have recently predicted six unexpected phases at 360 GPa for the Fe-Mg system. Their Fe_2Mg, $FeMg_2$, and $FeMg_3$ phases remain stable at 1 TPa, but all become unstable at 3 TPa [14]. Reference [14] gives a detailed discussion of the stabilities of the binary Fe-Mg phases. Here we use the structures of these unreported stable Fe-Mg compounds, i.e., Fe_2Mg_3, FeMg, Fe_3Mg_2, and $FeMg_2$, as the binary references under 3 TPa. Details of the space groups and lattice parameters of the above-mentioned elementary and binary phases are listed in Table S1 for 1 TPa and Table S2 for 3 TPa, respectively, in the Supplemental Material [39]. The crystal structures of all the stable elementary and binary phases on the convex hull at 1 and 3 TPa are displayed in Figs. S1 and S2, respectively, in the Supplemental Material [39].

Based on these elementary and binary references, we construct the Fe-Mg-O system's ternary phase diagrams and convex hull. As depicted in Fig. 1(a), the ternary phase diagram exhibits two stable stoichiometric Fe-Mg-O compounds at 1 TPa, namely, $FeMgO_3$ and $FeMg_3O_4$. These two structures remain the ground state at 3 TPa even though the binary references differ, as shown in Fig. 1(b).

B. Structural geometry

Figure 2 shows the predicted ternary $Fe_xMg_yO_z$ phases' ground-state structures (see Tables S3 and S4 in the Supplemental Material [39] for crystallographic details). The oxygen-rich $FeMgO_3$ phase is an orthorhombic structure with *Pnma* symmetry. As can be seen in Fig. 2(a), each Fe atom in the $FeMgO_3$ phase is coordinated to eight oxygen atoms, forming the Fe-centered FeO_8 cubes, while each Mg atom is coordinated to ten oxygen atoms, forming the MgO_{10} polyhedrons. By sharing their faces, the FeO_8 and MgO_{10} clusters constitute the *Pnma* phase of $FeMgO_3$. The $FeMg_3O_4$ phase adopts a cubic structure with $Im\bar{3}m$ symmetry. In the $FeMg_3O_4$ lattice [2 f.u. shown in Fig. 2(b)], Mg atoms occupy the edge centers and face centers, while Fe atoms are located at the corners and body centers. Both Mg and Fe are in the environment of FeO_8/MgO_8 cubes. To check if there is any disordered Mg/Fe occupation, we generate several structures with the same oxygen occupation but randomly permutated metal sites with Fe/Mg. We optimize these structures and find these structures all have larger enthalpy than the ground-state structure from the AGA search. The enthalpy difference ranges from 66 to 325 meV/atom.

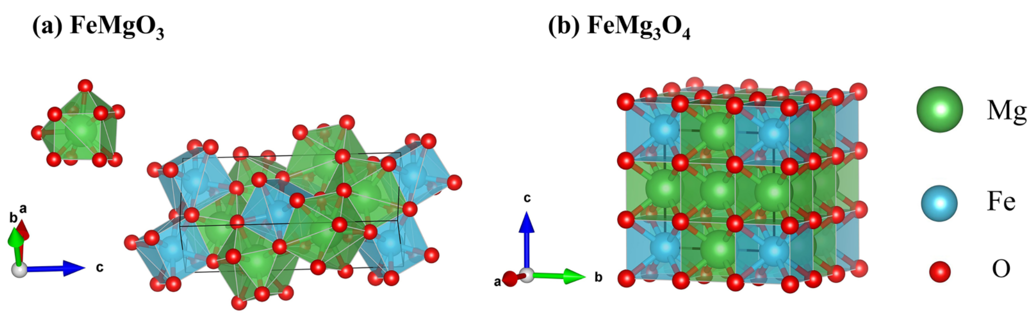

FIG. 2. Crystal structures of stable $Fe_xMg_yO_z$ phases: (a) *Pnma* $FeMgO_3$ and (b) $Im\bar{3}m$ $FeMg_3O_4$.

Both $FeMgO_3$ and $FeMg_3O_4$ show spin-unpolarized ground states and metallic behaviors at 1 and 3 TPa.

C. Local packing motifs

Since the effect of temperature is not considered in this paper, other structures metastable at $T = 0$ K may become stable at high temperatures. For this reason, we also investigate the AGA-searched $Fe_xMg_yO_z$ phases with relative enthalpies (ΔH) up to 0.8 eV/atom (≈9000 K) above the convex hull. These structures provide better statistics to explore further the impact of high pressure on the Fe-Mg-O system. We employ the cluster alignment (CA) method [40–42] to classify these metastable structures based on their local packing motifs. The clusters here are defined by a center atom and its first-shell neighbor atoms. In the CA analysis, a root mean squared deviation (RMSD) was used to describe the dissimilarity between an as-extracted cluster and the perfect template cluster, as

$$S = \min_\alpha \sqrt{\frac{1}{n}\sum_{i=1}^{n}\frac{(\boldsymbol{r}_{ci} - \alpha\boldsymbol{r}_{ti})^2}{(\alpha\boldsymbol{r}_{ti})^2}},$$

where n denotes the number of neighboring atoms in the template; $\boldsymbol{r}_{ci}$ and $\boldsymbol{r}_{ti}$ represent the atomic positions in the

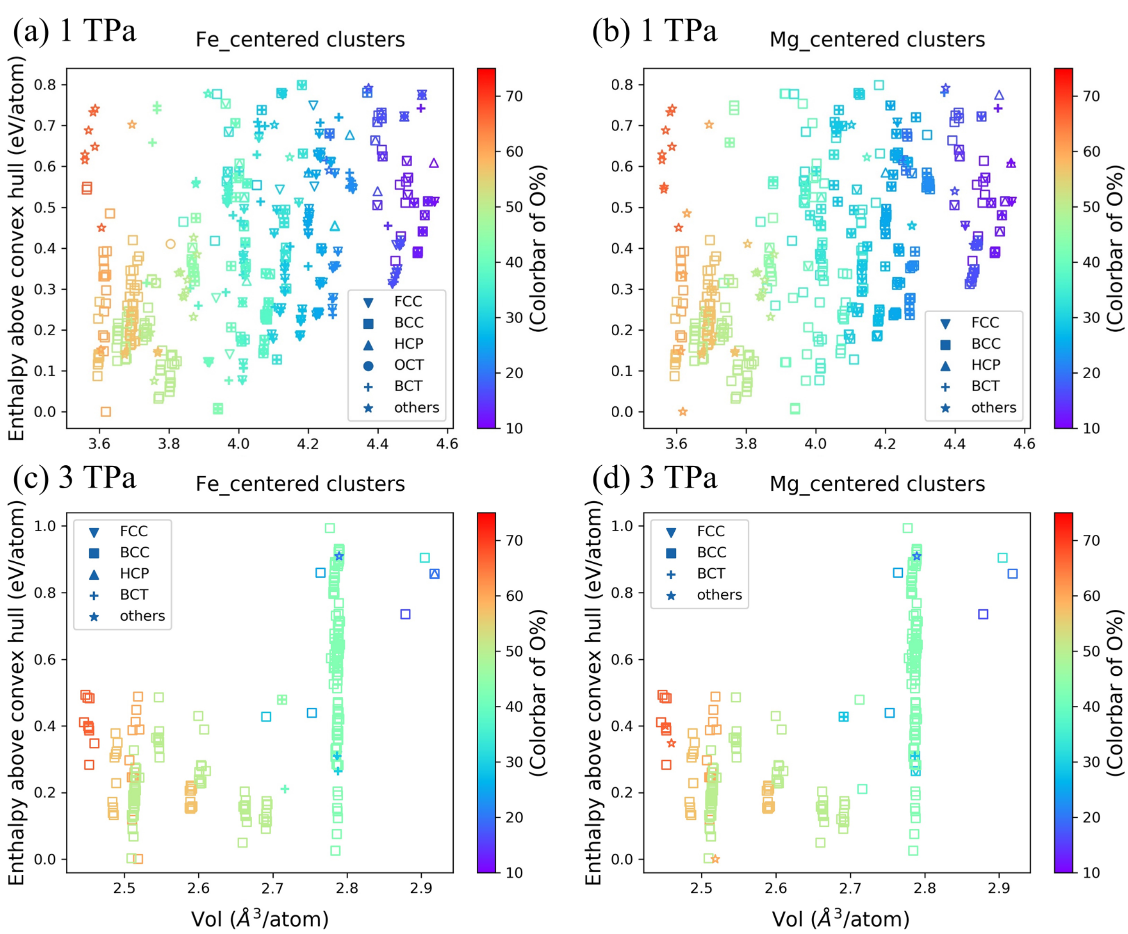

FIG. 3. The relative enthalpies of our predicted $Fe_xMg_yO_z$ structures as a function of their volumes, where the symbols indicate the local packing motifs, and the colors denote the oxygen concentration. (a), (b) Clusters with Fe and Mg as central atoms at 1 TPa, respectively. (c), (d) Clusters with Fe and Mg as central atoms at 3 TPa, respectively.

aligned clusters and template, respectively; and α is the optimal scaling parameter of the bond lengths in the template. Each as-extracted cluster from the sample is aligned to fcc, bcc, oct (octahedron), bct (body-centered tetragonal), and hcp templates, which are the most common motifs in the Fe-O and Mg-O system [9,34,35] as shown in Fig. S3 in the Supplemental Material [39]. The motif with the minimum RMSD out of these five templates is assigned to the cluster. If the lowest RMSD of the five templates are still higher than a criterion of 0.125, the cluster is classified as an unrecognized type (noted as "others" in the figures). This criterion is set for possible distortion of the perfect motifs in the crystal structures.

With the classified local motifs, Fig. 3 shows the scatter plot containing the information on the relative enthalpies with respect to the convex hull, the atomic volumes, the local packing motifs, and the oxygen concentrations for the stable and metastable phases. A similar plot with the mass densities is presented in Fig. S4 in the Supplemental Material [39] for the potential interest in the densities of these structures. Several conclusions can be drawn from Fig. 3. First, the averaged atomic volume directly correlates to the oxygen concentration. Higher oxygen concentration generally results in a smaller averaged atomic volume. Second, when comparing the low-energy structures among different oxygen concentrations, we find the oxygen-rich phases tend to be closer to the convex hull than the oxygen-poor phases at 1 TPa. A similar trend can be found at 3 TPa that the oxygen-poor phases have much higher energies above the convex hull, as shown in Figs. 3(c) and 3(d). By comparing the Fe- and Mg-centered motifs in Fig. 3, we find that Fe and Mg have very similar local motifs in most phases, even though they can have different coordination numbers. For example, while the Mg atoms in $FeMgO_3$ in Fig. 2(a) have higher coordination than Fe, it still adopts a distorted bcc motif. Therefore, CA provides more accurate descriptions of the local packing motifs than the coordination number. Finally, the bcc-type clusters dominate lower-energy structures, especially in the oxygen-rich low-enthalpy phases at both 1 and 3 TPa. This is consistent with the fact that both MgO and FeO adopt the B2 structure (bcc motif) under high pressures. The oxygen-poor phases with higher enthalpies show a mixture among bcc-, bct-, fcc-, and hcp-type clusters. It should be noted that although the octahedron motif is the only local packing motif in ferropericlase ($Mg_{1-x}Fe_xO$) at lower pressures within 100 GPa, it is very rare under current pressure conditions.

IV. CONCLUSIONS

In summary, we have investigated the structures and motifs of ternary $Fe_xMg_yO_z$ phases predicted by the adaptive genetic algorithm at 1 and 3 TPa. Two stable phases, namely, $FeMgO_3$ and $FeMg_3O_4$, are identified. The cluster alignment analysis reveals that bcc is the most favored packing motif for low-enthalpy Fe-Mg-O phases at these pressures. We also find that the oxygen-rich $Fe_xMg_yO_z$ phases generally have enthalpies closer to the convex hull than the oxygen-poor phases, suggesting that Mg-Fe cations are fully oxidized or nearly so at these high pressures and low temperatures. In this paper, we provide a comprehensive structure database to assist future efforts to study the high-pressure structural behaviors of Fe-Mg-O compounds.

ACKNOWLEDGMENTS

Work at Xiamen University was supported by the National Natural Science Foundation of China (Grants No. 12374015 and No. 42374108). Work at Iowa State University was supported by NSF Grant No. EAR-1918134. Work at Columbia University were supported by NSF Grants No. EAR-2000850 and No. EAR-1918126. Work at Guangdong University of Technology was supported by the Guangdong Basic and Applied Basic Research Foundation (Grants No. 2021A1515110328 and No. 2022A1515012174) and the Guangdong Natural Science Foundation of China (Grant No. 2019B1515120078). Work at Jimei University was supported by the Research Foundation of Jimei University (Grant No. ZQ2023013). Y.S. acknowledges support from the Fundamental Research Funds for the Central Universities (Grant No. 20720230014) and the Natural Science Foundation of Xiamen, China (Grant No. 3502Z202371007). Xiamen University's High-Performance Computing Center is acknowledged for its computational resources. Shaorong Fang and Tianfu Wu from Information and Network Center of Xiamen University are acknowledged for their help with GPU computing.

[1] M. Jura and E. D. Young, Extrasolar cosmochemistry, Annu. Rev. Earth Pl. Sc. **42**, 45 (2014).

[2] A. E. Doyle, E. D. Young, B. Klein, B. Zuckerman, and H. E. Schlichting, Oxygen fugacities of extrasolar rocks: Evidence for an Earth-like geochemistry of exoplanets, Science **366**, 356 (2019).

[3] A. P. van den Berg, D. A. Yuen, K. Umemoto, M. H. G. Jacobs, and R. M. Wentzcovitch, Mass-dependent dynamics of terrestrial exoplanets using *ab initio* mineral properties, Icarus **317**, 412 (2019).

[4] J. Liu, Y. Sun, C. J. Lv, F. Zhang, S. Y. Fu, V. B. Prakapenka, C. Z. Wang, K. M. Ho, J. Lin, and R. M. Wentzcovitch, Iron-rich Fe-O compounds at Earth's core pressures, Innovation **4**, 100354 (2023).

[5] K. Umemoto, R. M. Wentzcovitch, S. Q. Wu, M. Ji, C. Z. Wang, and K. M. Ho, Phase transitions in $MgSiO_3$ post-perovskite in super-Earth mantles, Earth Planet Sc. Lett. **478**, 40 (2017).

[6] M. H. Shahnas, R. N. Pysklywec, and D. A. Yuen, Penetrative convection in super-Earth planets: Consequences of $MgSiO_3$ postperovskite dissociation transition and implications for super-Earth GJ 876 D, J. Geophys. Res. Planets **123**, 2162 (2018).

[7] K. Umemoto and R. M. Wentzcovitch, Two-stage dissociation in $MgSiO_3$ post-perovskite, Earth Planet Sc. Lett. **311**, 225 (2011).

[8] K. Umemoto, R. M. Wentzcovitch, and P. B. Allen, Dissociation of $MgSiO_3$ in the cores of gas giants and terrestrial exoplanets, Science **311**, 983 (2006).

[9] H. Y. Niu, A. R. Oganov, X. Q. Chen, and D. Z. Li, Prediction of novel stable compounds in the Mg-Si-O system under exoplanet pressures, Sci. Rep. **5**, 18347 (2015).

[10] J. J. Wang, H. Gao, Y. Han, C. Ding, S. N. Pan, Y. Wang, Q. H. Jia, H. T. Wang, D. Y. Xing, and J. Sun, MAGUS: Machine learning and graph theory assisted universal structure searcher, Natl. Sci. Rev. **10**, nwad128 (2023).

[11] N. Dubrovinskaia, L. Dubrovinsky, I. Kantor, W. A. Crichton, V. Dmitriev, V. Prakapenka, G. Shen, L. Vitos, R. Ahuja, B. Johansson *et al.*, Beating the miscibility barrier between iron group elements and magnesium by high-pressure alloying, Phys. Rev. Lett. **95**, 245502 (2005).

[12] N. Dubrovinskaia, L. Dubrovinsky, and C. McCammon, Iron-magnesium alloying at high pressures and temperatures, J. Phys. Condens. Mat. **16**, S1143 (2004).

[13] P. Gao, C. Su, S. Shao, S. Wang, P. Liu, S. Liu, and J. Lv, Iron-magnesium compounds under high pressure, New J. Chem. **43**, 17403 (2019).

[14] Y. M. Fang, Y. Sun, R. H. Wang, F. Zheng, S. Q. Wu, C. Z. Wang, R. M. Wentzcovitch, and K. M. Ho, Unconventional iron-magnesium compounds at terapascal pressures, Phys. Rev. B **104**, 144109 (2021).

[15] T. Tsuchiya, R. M. Wentzcovitch, C. R. S. da Silva, and S. de Gironcoli, Spin transition in magnesiowustite in earth's lower mantle, Phys. Rev. Lett. **96**, 198501 (2006).

[16] Z. Wu, J. F. Justo, C. R. S. da Silva, S. de Gironcoli, and R. M. Wentzcovitch, Anomalous thermodynamic properties in ferropericlase throughout its spin crossover transition, Phys. Rev. B **80**, 014409 (2009).

[17] E. Holmstrom and L. Stixrude, Spin crossover in ferropericlase from first-principles molecular dynamics, Phys. Rev. Lett. **114**, 117202 (2015).

[18] T. Q. Wan, Y. Sun, and R. M. Wentzcovitch, Intermediate spin state and the *B*1-*B*2 transition in ferropericlase, Phys. Rev. Res. **4**, 023078 (2022).

[19] H. Hsu and K. Umemoto, Structural transition and re-emergence of iron's total electron spin in (Mg,Fe)O at ultrahigh pressure, Nat. Commun. **13**, 2780 (2022).

[20] F. Della Pia and D. Alfe, *B*1-*B*2 phase transition of ferropericlase at planetary interior conditions, Phys. Rev. B **105**, 134109 (2022).

[21] S. Q. Wu, M. Ji, C. Z. Wang, M. C. Nguyen, X. Zhao, K. Umemoto, R. M. Wentzcovitch, and K. M. Ho, An adaptive genetic algorithm for crystal structure prediction, J. Phys. Condens. Mat. **26**, 035402 (2014).

[22] D. M. Deaven and K.-M. Ho, Molecular geometry optimization with a genetic algorithm, Phys. Rev. Lett. **75**, 288 (1995).

[23] S. M. Foiles, M. I. Baskes, and M. S. Daw, Embedded-atom-method functions for the fcc metals Cu, Ag, Au, Ni, Pd, Pt, and their alloys, Phys. Rev. B **33**, 7983 (1986).

[24] X. Zhou, R. Johnson, and H. Wadley, Misfit-energy-increasing dislocations in vapor-deposited CoFe/NiFe multilayers, Phys. Rev. B **69**, 144113 (2004).

[25] A. Banerjea and J. R. Smith, Origins of the universal binding-energy relation, Phys. Rev. B **37**, 6632 (1988).

[26] P. Brommer and F. Gähler, Potfit: Effective potentials from *ab initio* data, Model Simul. Mater. Sci. Eng. **15**, 295 (2007).

[27] P. Brommer and F. Gähler, Effective potentials for quasicrystals from ab-initio data, Philos. Mag. **86**, 753 (2006).

[28] P. Giannozzi, S. Baroni, N. Bonini, M. Calandra, R. Car, C. Cavazzoni, D. Ceresoli, G. L. Chiarotti, M. Cococcioni, I. Dabo *et al.*, QUANTUM ESPRESSO: A modular and open-source software project for quantum simulations of materials, J. Phys. Condens. Mat. **21**, 395502 (2009).

[29] P. Giannozzi, O. Andreussi, T. Brumme, O. Bunau, M. B. Nardelli, M. Calandra, R. Car, C. Cavazzoni, D. Ceresoli, M. Cococcioni *et al.*, Advanced capabilities for materials modelling with QUANTUM ESPRESSO, J. Condens. Matter. Phys. **29**, 465901 (2017).

[30] J. P. Perdew, K. Burke, and M. Ernzerhof, Generalized gradient approximation made simple, Phys. Rev. Lett. **77**, 3865 (1996).

[31] K. Umemoto, R. M. Wentzcovitch, Y. G. Yu, and R. Requist, Spin transition in (Mg,Fe)SiO_3 perovskite under pressure, Earth Planet Sc. Lett. **276**, 198 (2008).

[32] F. Zheng, Y. Sun, R. H. Wang, Y. M. Fang, F. Zhang, B. Da, S. Q. Wu, C. Z. Wang, R. M. Wentzcovitch, and K. M. Ho, Structure and motifs of iron oxides from 1 to 3 TPa, Phys. Rev. Mater. **6**, 043602 (2022).

[33] J. Shi, W. Cui, S. Botti, and M. A. L. Marques, Nitrogen-hydrogen-oxygen ternary phase diagram: New phases at high pressure from structural prediction, Phys. Rev. Mater. **2**, 023604 (2018).

[34] G. L. Weerasinghe, C. J. Pickard, and R. J. Needs, Computational searches for iron oxides at high pressures, J. Phys. Condens. Mat. **27**, 455501 (2015).

[35] Q. Zhu, A. R. Oganov, and A. O. Lyakhov, Novel stable compounds in the Mg-O system under high pressure, Phys. Chem. Chem. Phys. **15**, 7696 (2013).

[36] P. F. Li, G. Y. Gao, Y. C. Wang, and Y. M. Ma, Crystal structures and exotic behavior of magnesium under pressure, J. Phys. Chem. C **114**, 21745 (2010).

[37] J. Sun, M. Martinez-Canales, D. D. Klug, C. J. Pickard, and R. J. Needs, Persistence and eventual demise of oxygen molecules at terapascal pressures, Phys. Rev. Lett. **108**, 045503 (2012).

[38] D. Vanderbilt, Soft self-consistent pseudopotentials in a generalized eigenvalue formalism, Phys. Rev. B **41**, 7892 (1990).

[39] See Supplemental Material at http://link.aps.org/supplemental/10.1103/PhysRevMaterials.7.113602 for the structural parameters of the stable elementary and binary phases in the Fe-Mg-O system at 1 and 3 TPa; crystal structures of the stable elementary and binary phases; crystallographic data of stable ternary Fe-Mg-O phases at 1 and 3 TPa; common motifs in Fe-O and Mg-O binary compounds; and the enthalpy versus density plot of the stable and metastable Fe-Mg-O structures at 1 and 3 TPa.

[40] Y. Sun, F. Zhang, Z. Ye, Y. Zhang, X. Fang, Z. Ding, C. Z. Wang, M. I. Mendelev, R. T. Ott, M. J. Kramer *et al.*, "Crystal genes" in metallic liquids and glasses, Sci. Rep. **6**, 23734 (2016).

[41] X. W. Fang, C. Z. Wang, Y. X. Yao, Z. J. Ding, and K. M. Ho, Atomistic cluster alignment method for local order mining in liquids and glasses, Phys. Rev. B **82**, 184204 (2010).

[42] S. Ren, Y. Sun, F. Zhang, A. Travesset, C. Z. Wang, and K. M. Ho, Phase diagram and structure map of binary nanoparticle superlattices from a Lennard-Jones model, ACS Nano **14**, 6795 (2020).